Measurement and Characterization of Various Outdoor 60 GHz Diffracted and Scattered Paths

Jonathan S. Lu[1,2], Patrick Cabrol[2], Daniel Steinbach[2] and Ravikumar V. Pragada[2]
Polytechnic Institute of New York University[1], InterDigital Communications LLC[2]
lushiaoen@gmail.com, Patrick.Cabrol@interdigital.com, Daniel.Steinbach@interdigital.com and
Ravikumar.Pragada@interdigital.com

***Abstract*— This paper investigates diffracted and scattered waves in unlicensed millimeter wave mobile-to-mobile, access and backhaul radio links. Narrowband 60 GHz measurements of diffraction at building corners, and scattering by a car, lamppost and building, as well as blocking by humans are presented. Semi-analytical corner diffraction and human blocking models are proposed and verified based on the measurements. Analysis of the diffraction and scattering shows that the contributions from vehicular and lamppost scattered paths can be dominant compared to corner diffracted paths. Measurements also show that the majority of power from building scattering arrives in and near the horizontal plane containing the transmit and receive antennas.**

Keywords—60 GHz; Backhaul; Diffraction; Millimeter Wave; mmW; Mobile-to-Mobile; IEEE 802.11ad; IEEE 802.11aj; NLOS; Scattering

I. INTRODUCTION

The 57–64 GHz millimeter wave (mmW) unlicensed band, also known as the 60 GHz band, allows for multi-gigabit data rates [1] with high spatial reuse. This has prompted the attention of short-range wireless personal area networks (WPAN) standards (e.g., Wireless HD, IEEE 802.15.3c and ECMA 387), and wireless local-area networks (WLAN) standards (e.g., WiGIG, IEEE 802.11ad and IEEE 802.11aj). Many indoor applications have been proposed, such as indoor cable-replacement for home and office multimedia streaming. Outdoor applications have also gained popularity. Currently backhaul is the predominant point-to-point outdoor use-case for mmW frequencies with the focus slowly moving towards mobile broadband systems. The 802.11ad standard allows for multiple simultaneous direct mobile-to-mobile communications [2]. It is envisioned that in mmW mobile wireless systems, mmW cells can be deployed utilizing existing street furniture, building corners or building surfaces avoiding the need for expensive dedicated mmW cell towers.

There is a plethora of literature summarized in [3], [4] on the wideband and narrowband channel parameters of 60 GHz indoor links. In comparison, there is a smaller amount of applicable literature [5], [6] on the channel parameters of 60 GHz outdoor radio links and even fewer on the site-specific interactions with common outdoor radio link obstructions (e.g., buildings and cars). In [5] and [6], it was found that there was large variability in the channel parameters due to these site-specific features. Understanding the strong dependence of the channel parameters on these features requires further investigation into the propagation characteristics of the individual obstructions.

Whether a mmW system has sufficient SNR for a non-line-of-sight (NLOS) link where one end of the radio link is shadowed is dependent on the rays propagating around and through the obstruction. For shadowing by a building, transmission loss through building materials at 60 GHz is very high [7], so it is expected that the diffraction at the building corner and scattering from objects near the corner will be the dominant modes of propagation. Diffraction of simple objects such as wooden and metal blocks [8] has been studied, but to the best of the authors' knowledge, there are no 60 GHz measurements characterizing building corner diffraction. Therefore, we have made measurements on corner diffraction and found that an absorbing screen diffraction coefficient best models our measurements.

For human shadowing, significant fades up to 50 dB [9] have been observed. Thus human blockers must be accounted for in RF prediction tools. Human blockers have been modeled as finite absorbing screens [8], [9], and water cylinders [10]. Verification of these models has generally only been done for a single mobile-to-mobile blocker scenario. In this work, we further verify the absorbing screen model for multiple humans blocking a mobile-to-mobile and a single human blocking an access link using uniform theory of diffraction (UTD) and physical optics.

For line-of-sight (LOS) communications, propagation paths other than the LOS path may need to be used because of temporary obstructions such as the aforementioned human blocking. In [5], it was found that NLOS paths near the LOS path generally had smaller delay spread and less loss relative to the LOS. These NLOS paths may arise from scattering from lamppost and other street furniture. Similarly for NLOS communications caused by building shadowing, this street furniture may give significant contributions for turning a corner as observed in UHF communications [11]. We have therefore performed a 60 GHz empirical study on vehicular, lamppost and building scattering.

Section II describes our measurement setup and scenarios. Simple diffraction models used to compare with our measurements are given in Section III. The measurements are presented and analyzed, and compared with the models of Section II in Section IV.

978-0-7695-5124-1/13 $31.00 © 2013 IEEE
DOI 10.1109/MILCOM.2013.212

II. Measurement Setup and Procedure

For all of our 60 GHz measurement scenarios, the same measurement equipment was used to record the received power. In the individual scenarios, the antenna heights and positioning varied as discussed below.

A. Measurement Equipment Setup

A diagram of our 60 GHz measurement equipment setup is shown in Fig. 1. In the transmit system (TX), the SMF100A microwave signal generator provides a 10 GHz sine wave to the SMZ90 frequency multiplier, which multiplies the frequency by six. The resulting 60 GHz signal then travels through a straight section waveguide to the V-band horn antenna with 24 dBi of gain and an 11 degree 3 dB beamwidth whose normalized antenna pattern is shown in Fig. 2. In the receive system (RX), the signal is received with an identical horn antenna that is connected to the N12-3387 low noise amplifier (LNA) with a straight waveguide section. The amplified signal is sent to the FS-Z90 harmonic mixer where it is down-converted and captured on the FSQ26 vector signal analyzer (VSA).

B. Measurements from Building, Car, and Lamppost

To perform outdoor measurements on buildings, cars, and lampposts shown in Fig. 3, the transmit (TX) and receive (RX) systems illustrated in Fig. 1, were each placed on push carts. To accurately point the antennas, the antennas were placed on pan-tilt motors of 0.0032° angle resolution, which were attached to the carts. Laptops on both carts ran a C++ program that was developed to control the motors, query the VSA for the received signal power and store measurement data.

The antennas' heights h_{TX} and h_{RX} relative to the ground for these measurement scenarios were 1.33 m and characterize a mobile-to-mobile radio scenario. Because the building scattering measurements were performed for sufficiently short link lengths in which the contribution from ground reflections was severely attenuated by the antenna pattern, these measurements should also apply to backhaul radio links. To apply the diffraction results to access links, an additional cosine angle dependence should be included [12] to account for the oblique incidence caused by the height difference.

1) Building Corner: To investigate the path loss for a NLOS link in which the RX is shadowed by a building, diffraction measurements around two different corners were recorded. The geometries of the corners are shown in Fig. 4. The first corner considered was composed of concrete. The TX cart was placed so that the TX distance from the corner r_{TX} = 3.75 m and φ' = 18 degrees. The RX was moved in an arc in the shadowed region. The radius of the arc which is the distance to the corner r_{RX} = 2.8 m. Measurements were recorded for angles φ = 200 to 260 degrees at intervals of 10 degrees.

Measurements were also performed on another corner shown in Fig. 3.a, composed of concrete with windows located near the corner. The TX cart was placed so that r_{TX} = 6.1 m and φ' = 10 degrees. The RX was again moved in an arc with radius r_{RX} = 4.0 m in the shadow region. Measurements were recorded for φ = 200 to 260 degrees at intervals of 15 degrees.

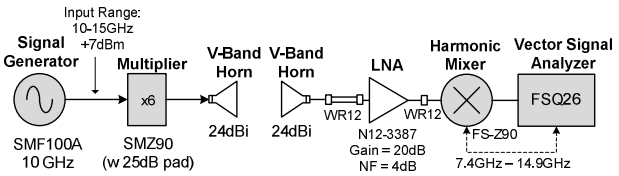

Figure 1. Block diagram of 60 GHz measurement setup

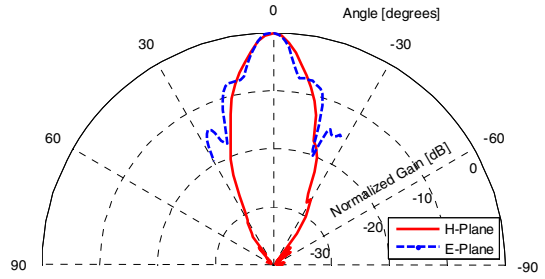

Figure 2. H-Plane and E-Plane normalized antenna gains.

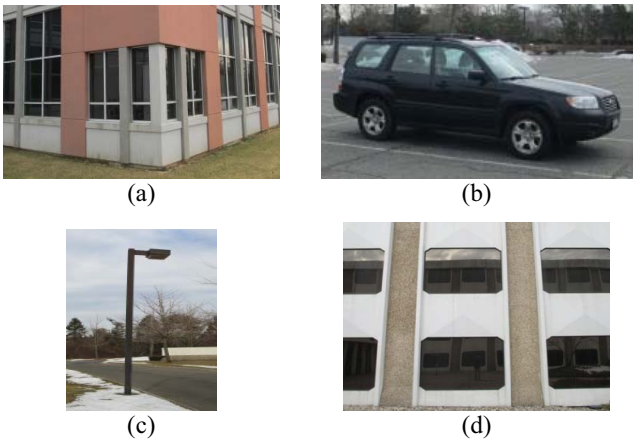

(a) (b) (c) (d)

Figure 3. (a) Corner 2, (b) Car, (c) Lamppost and (d) Building

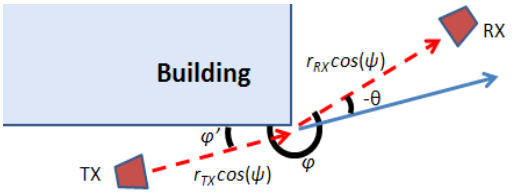

Figure 4. Diffraction around a building corner.

2) Car: Vehicular scattering measurements on a 2006 Subaru Forrestor shown in Fig. 3.b, were recorded in an empty parking lot. The TX antenna was placed at distance r_{TX} = 23 m from the car. The TX antenna bore sight was centered on the side of the car and was normal (θ_i = 0 degrees) to the car's surface. Measurements were recorded as the RX antenna was moved in an arc of approximate radius r_{RX} = 23 m, so that the scattering angle θ_s relative to the normal of the car surface, spanned 14 to 75 degrees.

3) Lamp Post: Power measurements on an isolated 3.7 m high lampost shown in Fig. 3.c, with a square 0.1 m x 0.1 m cross section were performed. The TX antenna was placed at a distance r_{TX} = 5 m from the lamppost. Measurements were recorded as the RX antenna was moved in an arc of radius r_{RX} = 5.5 m around the lampost so that the angle between the incident and scattered ray ψ_s spanned 7 to 151 degrees.

4) Building Surface: To investigate the reflection/scattering of features on a building surface, power angle profile measurements from a 4-story office building shown in Fig. 3.d, were performed. The TX and RX antennas were placed so that they were separated from each other by 8 m, and were 8.5 m from the building surface. Using the pan-tilt motors the TX antenna illuminated different portions of the building surface. For each portion of the building surface, the RX antenna illuminated the same surface, so as to measure the received power from that surface.

C. Human Blocking Measurements

Human blocking measurements were performed for mobile to mobile and access link scenarios. These measurements are later compared with predictions found from assuming the blockers are absorbing screens and then using UTD and physical optics to compute the diffraction loss.

1) Mobile to Mobile: In mobile to mobile communications the TX and RX antennas are typically at the same height or lower than normal human height. From [8], the majority of human blocking cases involved three blockers at most. Thus, we investigated two and three human blocking scenarios of a 7 m LOS link. The antenna heights were $h_{TX} = h_{RX} = 1$ m. A more detailed presentation of the setup and results is found in [9].

2) Access: For office or outdoor access radio links, the TX antennas are typically located on ceilings, light posts, etc., above human height. To investigate this radio scenario, one human blocking measurements of a 7 m LOS link were performed. The antenna heights were h_{TX} = 2.65 m and h_{RX} = 0.9 m. Measurements were recorded as the human blocker moved from the TX toward the RX antenna. During the entire experiment, the human blocker's body faced the RX antenna and was centered on the direct line between the TX and RX antenna.

For each of the mobile-to-mobile and access link human blocking configurations, five measurements were recorded over a 5 second time period. These measurements were then time-averaged in an attempt to mitigate the inadverdent movement of the human blockers.

III. Diffraction From Single and Multiple Edges

A diffracting corner is modeled as a conducting right-angle wedge and an absorbing screen with a knife-edge in our comparison with measurements. Human blockers are modeled as semi-infinite absorbing screens with knife-edges. The following sub-sections give expressions for the path gain and diffraction loss around a conducting wedge, and single and multiple absorbing screens.

A. Diffraction Around a Single Edge

The received power P_R in watts from diffraction around a vertical edge [12] can be expressed in the form

$$P_R = P_T G_{RX} G_{TX} \left(\frac{\lambda}{4\pi(r_1 + r_2)} \right)^2 \left[\frac{\left| D(\varphi, \varphi') \right|^2}{\cos^2(\psi)} \frac{r_1 + r_2}{r_1 r_2} \right]. \quad (1)$$

Here P_T is the transmitted power in watts, and G_{RX} and G_{TX} are the antenna gains of the TX and RX antennas, respectively. λ is the wavelength in meters, φ and φ' are the angles in radians defined in Fig. 4, $\pi/2 - \psi$ is the acute angle the incident wave makes with the edge in radians, and $D(\varphi, \varphi')$ is the diffraction coefficient. Note that when $\psi = 0$, the incident wave is incident normal to the edge. r_1 and r_2 are the distances of the TX and RX antennas to the edge in meters, respectively. The received power can be separated into two terms. The first term is the LOS power along the diffracted path. The second term in the square bracket is the diffraction loss incurred from diffracting around the corner.

For a semi-infinite absorbing screen with a knife edge corner, the UTD expression for $D(\varphi, \varphi')$ is

$$D(\theta) = -\frac{\sqrt{2\pi S}}{\sqrt{2\pi k}} \frac{1 + \cos(\theta)}{2\sin(\theta)} \left[f\left(\sqrt{\frac{2S}{\pi}} \right) + jg\left(\sqrt{\frac{2S}{\pi}} \right) \right]. \quad (2)$$

Here $\theta = \pi + \varphi' - \varphi$ as seen in Fig. 4, and f, g, and S are defined in [12, chapter 5].

For a conducting right angle wedge corner with E-field parallel to the edge, the geometric theory of diffraction (GTD) diffraction coefficient is expressed as

$$D(\varphi, \varphi') = \frac{-1}{3\sqrt{2\pi k}} \left[\cot\left(\frac{\pi + (\varphi - \varphi')}{3} \right) + \cot\left(\frac{\pi + (\varphi + \varphi')}{3} \right) - \cot\left(\frac{\pi - (\varphi - \varphi')}{3} \right) - \cot\left(\frac{\pi - (\varphi + \varphi')}{3} \right) \right]. \quad (3)$$

B. Diffraction Around Multiple Absorbing Screens

To compute the diffraction loss, defined as free-space power to diffracted power, from an arbitrary number of screens parallel to the $y = 0$ plane, we use a physical optics method developed by Piazzi [12]-[14]. This method is based on the same principles of physical optics used in [15].

Assuming a) the knife-edges are of infinite length and are parallel, and b) the additional diffraction loss for a point source on a plane that is perpendicular to the screens is the same as that for a line source that is parallel to the screens and intersects the plane at the source point, the physical optics description of diffraction around an absorbing screen is expressed as multiple integrations in the x–z planes containing the absorbing screens. The integrations in the coordinate along a z-plane knife-edge can be approximated analytically so that we are left with integration in the x-coordinate away from the knife-edges. This is seen in the following expression for the magnetic field $H(x_{n+1}, y_{n+1})$ in the plane containing the $n + 1$ absorbing screen [13]:

$$H(x_{n+1}, y_{n+1}) = e^{j\pi/4}\sqrt{\frac{k}{2\pi}}\int_{-\infty}^{\infty} H(x_n, y_n)\frac{e^{-jk\rho}}{\sqrt{\rho}}dx_n \,. \qquad (4)$$

Here ρ is the distance from the secondary source point (x_n, y_n) on plane $x = x_n$ to receiver point (x_{n+1}, y_{n+1}) on plane $x = x_n+1$, and k is the free-space wave number. The field on plane x = x_n containing the nth screen is given by $H(x_n, y_n)$. To arrive at an expression with multiple integrals, we substitute $H(x_n, y_n)$ in (4) with $H(x_{n-1}, y_{n-1})$, which is the field on plane $x = x_{n-1}$ containing the *n - 1* screen and can similarly be written in integral form.

To predict the diffracted power from multiple screens, the integrals must be carried out numerically. The integral in (4) must be terminated with finite upper and lower limits (for the right and left sides of the screen), and the integration must be replaced by a discrete summation. The Piazzi method involves simple linear approximations of the amplitude and phase and introduces a smoothing procedure that uses a Kaiser-Bessel function to terminate the integration without introducing spurious diffraction [12]–[14].

IV. Results and Analysis

The recorded measurements are presented and compared with theoretical models in this section.

A. Building Corner Diffraction

The magnitude of the diffraction coefficient values are computed from building corner measurements using (1), and are plotted in dB versus θ = π + φ' - φ in Fig. 5. Also plotted are the UTD absorbing screen diffraction coefficient (2) and the conducting GTD right-angle wedge diffraction coefficients (3) for φ' = 10 and 18 degrees. As seen in Fig. 5, the conducting wedge gives a pessimistic prediction to the diffraction coefficient, while the absorbing screen gives a more reasonable prediction. To quantify the accuracy we define the error as the predicted diffraction coefficient magnitude in dB minus the measured. The absorbing screen diffraction coefficient for φ' = 10 and 18 degrees gives mean errors of -1 and 2.79 dB, respectively. The standard deviations of error are 1.56 and 2.6 dB respectively.

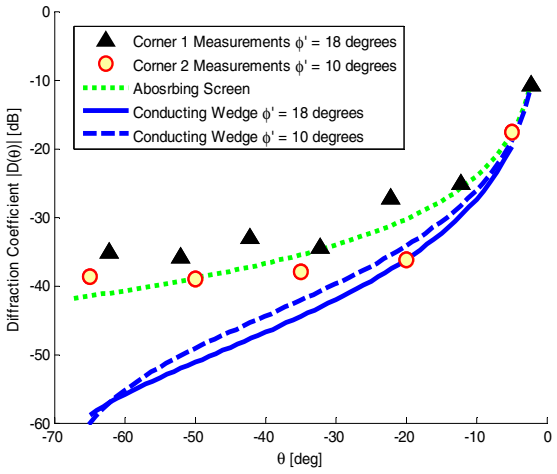

Figure 5. Comparison of diffraction coefficient measurements and theoretical diffraction coefficients.

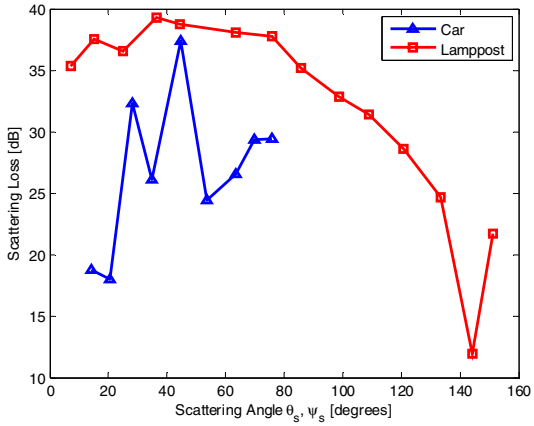

Figure 6. Scattering loss from a car with incident angle θ_i = 0 degrees, and lamppost.

From [16], the structure of a diffracting corner has a significant impact on the diffraction coefficient of the corner. For example, rays traveling through the windows near to a corner may have a larger contribution to the received power than those diffracted by the corner. In our measurements, we did not see this effect probably because the metal blinds of the windows near the corner shown in Fig. 3.c were drawn down.

B. Scattering from Car and Lampost

The scattering losses from a car (blue triangles) are plotted versus scattering angle θ_s in Fig. 6. The scattering loss is the received power normalized to the free space power over the scattering path length $r_{TX} + r_{RX}$. As expected, the scattering loss is smaller nearer to the specular direction θ_s = 0 degrees.

The scattering losses from a lamppost (red squares) are plotted versus the scattering angle ψ_s between the incident and reflected waves in Fig. 6. Again, the scattering loss is the received power normalized to the free space power over the scattering path length $r_{TX} + r_{RX}$. The low loss at 144 degrees on the lamppost curve corresponds to specular reflection from the lamppost's rectangular cross section.

C. Building Shadowing; Diffraction vs. Scattering

It is interesting to compare the contributions from scattered rays and diffracted rays for the case of a NLOS mmW link in which the TX and RX are located on the sidewalks of adjacent sides of a building, and $r_{TX} = r_{RX}$ = 23m from the corner. The diffraction angle θ is then close to -90 degrees, so that the absorbing screen diffraction coefficient magnitude is approximately 40 dB. Accounting for the distance dependence, the diffraction loss (square brackets of (1)) is then approximately 50 dB. Now assume there is a car near the corner and the car is parked parallel to the building surface. Using our measurements from Fig. 6, the scattering loss is then on the order of 30 dB. For this case the vehicular scattering gives a much larger contribution than the corner diffraction.

Now consider a similar case, but with a square cross-section lamppost near the corner instead of a car and the RX and TX distances to the corner and lamppost are r_{TX} = 5 m and r_{RX} = 5.5 m, respectively. The diffraction loss for the corner is 44 dB, while the scattering loss from Fig. 6, will be less than 40 dB. Depending on how the lamppost is oriented, the

scattering loss can be on the order of 12 dB. Thus, for this scenario, the contribution from the lamppost is expected to be dominant.

To extend these results to more general radio scenarios, we would have to know the distance dependence of the received power from the car and lamppost. Though, if we assume they have similar distance dependence to corner diffraction, we can conclude that the scattering will usually be dominant for the short TX-RX separations under consideration.

D. Building Scattering

The received power angular profile minus the LOS power in dBm at the RX antenna is plotted in Fig. 7. It can be seen that the majority of power arrives in the horizontal plane (elevation angle = 0 degrees) containing the TX and RX antennas at 0, 25 and 40 degrees. The 0 and 40 degree humps correspond to columns on the building surface, while the 25 degree hump corresponds to specular reflection. Other humps outside this plane correspond to window sills and a triangular prism feature on the building surface. Other results not shown give similar results. These 60 GHz results are similar to UHF band results presented in [17] and [18], where the features on the building surface (e.g., balconies and columns) contributed significantly to the received power angle profile.

E. Mobile to Mobile Link Human Blocking

In our measurements, the transmission loss through a single blocker is greater than 50 dB, and reflection and scattering from nearby objects are heavily attenuated by the TX and RX antenna patterns. Therefore, the blocking loss, defined as the power ratio between the unobstructed to the obstructed received power, is essentially the diffraction loss around the blockers. In this sub-section, our mobile-to-mobile human blocking loss measurements are compared with diffraction loss predictions found using the Piazzi method described in Section III.B for human blockers modeled as semi-infinite absorbing screens of infinite height similar to [8], [19].

Fig. 8 shows the time-averaged blocking loss measurements for different two and three-person blocking configurations in increasing order of blocking loss. The predicted blocking losses from the Piazzi method are also plotted. Depending on the configuration of the blockers, there can be deep fades in the measurements where the blocking loss is greater than 30 dB. The blocking loss in all scenarios ranges from -2.7 dB to 43.5 dB. This range is much larger than those presented in [8] and [10] and further justifies the need to include human blocking models in 60 GHz channel simulators. Fig. 8 also shows the errors in the predictions made using the Piazzi method for the different blocking configurations. Prediction error is defined as the predicted blocking loss minus the time-averaged blocking loss. The mean and standard deviations of the prediction error are -1 dB and 5.2 dB, respectively. 70% of the configurations had prediction error between ±5 dB. The majority of configurations with high blocking loss typically have large positive prediction errors. High blocking loss may be caused by large diffraction angles. This suggests that another model, for example, a cylindrical model, may better predict diffraction around blockers at large diffraction angles. However, from the standard deviation, we expect that the absorbing-screen model is sufficient to compute blocking loss in most applications.

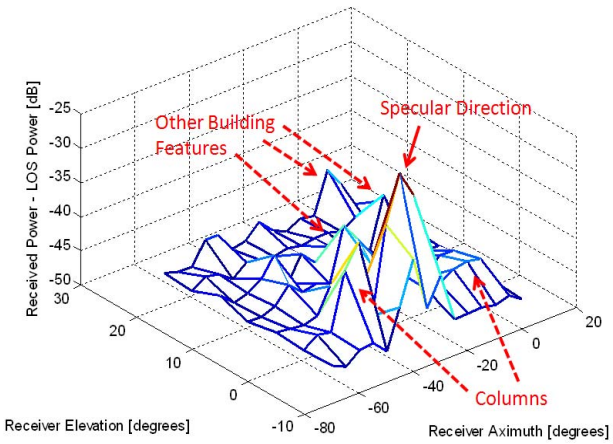

Figure 7. RX antenna received power angular profile relative to LOS power with incident angle $\theta_i = 25$ degrees on building.

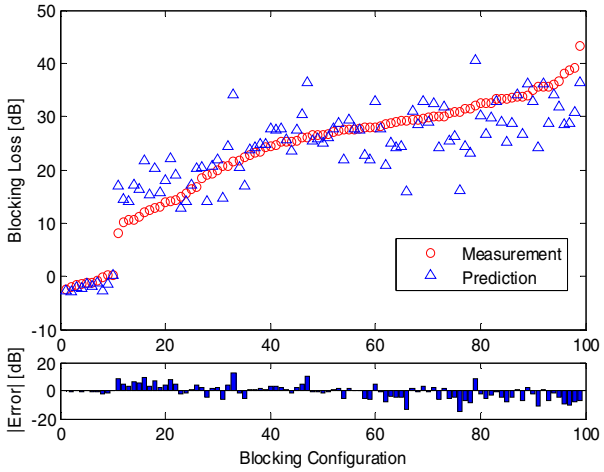

Figure 8. Comparison of mobile-to-mobile blocking gain measurements to Piazzi method predictions.

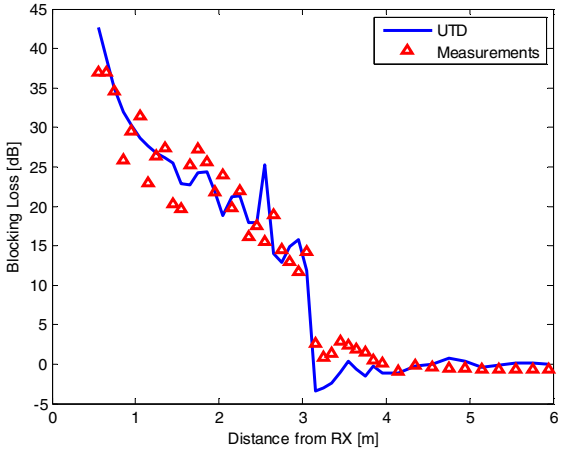

Figure 9. Comparison of access link blocking loss measurements to UTD predictions.

F. Access Link Human Blocking

The time-averaged blocking loss measurements as a human blocker walks toward the elevated TX antenna and away from the RX antenna is plotted in Fig. 8 versus the distance x from the TX antenna. To predict the blocking loss, the contributions from transmission through the humans, and scattering and reflection from nearby objects are again heavily attenuated, so that the blocking loss is the diffraction loss. Similar to the mobile-to-mobile case, two rays diffracting around the sides of the human blocker were considered. Unlike the mobile-to-mobile case, the absorbing screen modeling the blocker has finite height, because the antennas are no longer low relative to the blocker height. The predicted diffraction loss using the human blocker's actual width of 0.43 m and an effective height of 1.61 m for the absorbing screen is also plotted in Fig. 9. This effective height value was chosen so that mean prediction error was approximately 0 dB, which corresponded to a standard deviation of 3.2 dB.

Note that the actual height of the blocker is 1.72 m with a head height of 0.25 m. From this and other access link blocking measurements, we found that decreasing the blocker's head height by 35% to 45% gave the best prediction.

V. Conclusion

In this work, 60 GHz measurements of corner diffraction, scattering from a car, lamppost and building, and human blocking are presented. The absorbing screen diffraction model is found to give good comparison with diffraction measurements. Scattering measurements from cars and lampposts are found to peak near the specular direction. For building shadowed mmW links, comparisons of the scattering measurements with the absorbing screen diffraction model suggests that the scattering from cars and lampposts is dominant compared to corner diffraction. This indicates the need to include scattering models of common urban furniture in millimeter wave propagation simulators.

The building scattering measurements show that the majority of received power arrives in the horizontal plane containing the TX and RX and peaks in the specular direction. Non-specular contributions were found to originate from features on the wall, such as ridges and columns. Based on this result, we suggest utilizing a horizontal plane assumption in smart beam-finding algorithms when searching for building scattered paths to decrease complexity and acquisition time.

To account for human blocking in mmW propagation simulators, several models were previously proposed in the literature. In this work, we focused on the absorbing screen model and proposed the use of an effective human height for the screen height rather than the actual human height. Validation of this absorbing screen model was performed using human blocking measurements of single and multiple human blockers of mobile-to-mobile and access links. Results show that the absorbing screen model is quite accurate with standard deviation of prediction error less than 5 dB.

References

[1] R. C Daniels, J. N. Murdock, T. S. Rappaport and R. W. Heath Jr., "60GHz Wireless: Up close and Personal", *IEEE Microwave Mag*., Dec. 2010, pp. S44-S50,.

[2] 802.11ad-2012- IEEE Standard for Information technology-Tele-communications and information exchange between systems-Local and metropolitan area networks--Specific requirements-Part 11: Wireless LAN Medium Access Control (MAC) and Physical Layer (PHY) Specifications Amendment 3: Enhancements for Very High Throughput in the 60 GHz Band

[3] S. Yong, P. Xia, and A. Valdes-Garcia. *60GHz Technology for Gbps WLAN and WPAN: From Theory to Practice*. West Sussex, U.K: Wiley, 2011.

[4] J. Wells, *Multigigabit Microwave and Millimeter-Wave Wireless Communications*. Norwood, MA : Artech House, 2010.

[5] T. S. Rappaport, E. Ben-Dor, J. N. Murdock, and Y. Qiao, "38 GHz and 60 GHz Angle-Dependent Propagation for Cellular & Peer-to-Peer Wireless Communications," in *Proc. IEEE International Conference on Communications (ICC 2012)*, June 2012, pp. 4568-4573.

[6] E. Ben-Dor, T. S. Rappaport, Y. Qiao, and S. J. Lauffenburger, "Millimeter-wave 60 GHz Outdoor and Vehicle AOA Propagation Measurements using a Broadband Channel Sounder" in *Proc. IEEE Global Communications Conf. (Globecom)*, December 2011, pp. 1-6.

[7] C.R. Anderson and T. S. Rappaport, "In-building wideband partition loss measurements at 2.5 and 60 GHz," *IEEE Tran. on Wireless Communications*, vol. 3, No. 3, pp. 922-928, 2004.

[8] M. Jacob, S. Priebe, R. Dickhoff, T. Kleine-Ostmann, T. Schrader, T. Kürner, "Diffraction in mm and sub-mm Wave Indoor Propagation Channels", in *IEEE Trans. on Microwave Theory and Techniques*, Vol. 60, No. 3, pp.833-844, Mar. 2012.

[9] J. S. Lu, D. Steinbach, P. Cabrol, and P. Pietraski, "Modeling the Impact of Human Blockers in Millimeter Wave Radio Links" in *ZTE Communications Magazine*, Vol. 10, No. 4, pp. 23-28, Dec. 2012

[10] A. Khafaji, R. Saadane, J. El Abbadi and M. Belkasmi, "Ray tracing technique based 60 GHz band propagation modelling and influence of people shadowing" World Academy of Science, Engineering and Technology, 2008.

[11] M. Ghoraishi, J. Takada, T. Imai, "Identification of Scattering Objects in Microcell Urban Mobile Propagation Channel," *IEEE Trans. on Antennas and Propagation*, Vol. 54, No. 11, pp. 3473-3480, Nov. 2006.

[12] H.L. Bertoni, *Radio Propagation for Modern Wireless Applications*. Upper Saddle River, NJ: Prentice Hall, PTR, 2000.

[13] L. Piazzi, "Multiple Diffraction Modeling of Wireless Propagation in Urban Environments", Dissertation for the PhD Degree in ECE, 1998.

[14] L. Piazzi and H. L. Bertoni, "Effect of terrain on path loss in urban environments for wireless applications;" *IEEE Trans. on Antennas and Propagation*, vol. 46, No. 8, pp. 1138-1147, 1998.

[15] L. E. Vogler, "An attenuation function for multiple knife-edge diffraction," *Radio Science*, Vol. 17, No. 6 pp. 1541-1546, 1982.

[16] H.M. El-Sallabi, G. Liang, H.L. Bertoni, I.T. Rekanos, P. Vainikainen, "Influence of diffraction coefficient and corner shape on ray prediction of power and delay spread in urban microcells," *IEEE Trans. on Antennas and Propagation*, Vol. 50, No. 5, pp.703-712, May 2002.

[17] M.R.J.A.E. Kwakkernaat and M.H.A.J. Herben, "Diagnostic analysis of radio propagation in UMTS networks using high-resolution angle-of-arrival measurements," in *IEEE Antennas and Propagation Mag.*, Vol. 53, No. 1, pp. 66-75, Feb. 2011.

[18] E. M. Vitucci, F. Mani, V. Degli-Esposti, and C. Oestges, "Polarimetric properties of diffuse scattering from building walls: Experimental parameterization of a ray-tracing model," in *IEEE Trans. Antennas and Propagation*, Vol. 60, No. 6, pp. 2961-2969, June 2012.

[19] Kunisch and J. Pamp, "Ultra-wideband double vertical knife-edge model for obstruction of a ray by a person", in *Proc. IEEE ICUWB*, Sept. 2008.